Author Manuscript

Author Manuscript

Author Manuscript

Author Manuscript

HHS Public Access

Author manuscript

Nat Chem Biol. Author manuscript; available in PMC 2010 December 01.

Published in final edited form as:

Nat Chem Biol. 2010 June ; 6(6): 424–432. doi:10.1038/nchembio.368.

Endoplasmic Reticulum Ca^{2+} Increases Enhance Mutant Glucocerebrosidase Proteostasis

Derrick Sek Tong Ong[1], **Ting-Wei Mu**[1], **Amy E. Palmer**[2], and **Jeffery W. Kelly**[1,*]

[1]Departments of Chemistry and Molecular and Experimental Medicine, The Skaggs Institute for Chemical Biology, The Scripps Research Institute, La Jolla, CA 92037

[2]Department of Chemistry and Biochemistry, University of Colorado, Boulder, CO 80309

Summary

Altering intracellular calcium levels is known to partially restore mutant enzyme homeostasis in several lysosomal storage diseases, but why? We hypothesize that endoplasmic reticulum (ER) calcium level increases enhance the folding, trafficking and function of these mutant misfolding/degradation-prone lysosomal enzymes by increasing chaperone function. Herein, we report that increasing ER calcium levels by reducing ER calcium efflux through the ryanodine receptor (antagonists or RNAi) or by promoting ER calcium influx by SERCA2b overexpression enhances mutant glucocerebrosidase (GC) homeostasis in Gaucher's disease patient-derived cells. Post-translational regulation of the calnexin folding pathway by increasing the ER calcium concentration appears to enhance the capacity of this chaperone system to fold mutant misfolding-prone enzymes, increasing the folded mutant GC population that can engage the trafficking receptor at the expense of ER-associated degradation, increasing the lysosomal GC concentration.

Introduction

The proteome is maintained by the protein homeostasis, or proteostasis, network1—comprising ribosomal protein synthesis, chaperone- and enzyme-mediated protein folding2-4, vesicular trafficking, and protein degradation5 pathways, among others. Stress-responsive signaling pathways match proteostasis capacity to demand in subcellular compartments, including the cytosol6,7 and the endoplasmic reticulum (ER)8,9, by inducing a transcriptional program. Since we are constantly challenged by extrinsic (e.g., viral infections) and intrinsic stresses (e.g., inherited mutations) that usurp proteostasis capacity10, substantial efforts have been channeled into understanding the molecular underpinnings of the proteostasis network and how we can adapt it through stress-responsive signaling pathways to treat a variety of diseases1,11-15. For example, small molecule

Users may view, print, copy, download and text and data- mine the content in such documents, for the purposes of academic research, subject always to the full Conditions of use: http://www.nature.com/authors/editorial_policies/license.html#terms

* To whom correspondence should be addressed. Telephone: 858-784-9605 Fax: 858-784-9610 jkelly@scripps.edu.

Author contributions D.S.T.O. performed the majority of the experiments, analyzed the data, and wrote the initial draft of the paper. T-W.M. performed the initial dantrolene experiments and all the Ca^{+2} measurement experiments, and collaborated on the analysis of the data. The ER Ca^{+2} levels were measured in the A.E.P. laboratory. J.W.K. supervised the work and managed the final publication.

Competing Financial Interests Jeffery W. Kelly is a co-founder, shareholder and paid consultant for Proteostasis Therapeutics, Inc., and while this company is not currently pursuing any lysosomal storage diseases, that could happen in the future.

Author Manuscript Author Manuscript Author Manuscript Author Manuscript

proteostasis regulators that activate the unfolded protein response stress-responsive signaling pathway have been introduced to ameliorate lysosomal storage diseases (LSDs)13.

Lysosomal storage diseases are loss-of-function diseases, often caused by the inability of mutant lysosomal enzymes to fold in the ER at pH 716-19, rendering them susceptible to ER-associated degradation (ERAD)20, leading to accumulation of the enzyme's substrate in the lysosome16,17,21,22. Many Gaucher's disease (GD)-associated mutant enzymes exhibit sufficient stability and activity in the lysosome, provided they can fold in the ER and be trafficked to the lysosome23. Although LSDs are currently treated by enzyme replacement therapy, this approach is not applicable to neuropathic LSDs, as recombinant enzymes cannot cross the blood-brain barrier24. Pharmacologic chaperones, small molecules that bind to and stabilize the folded state of a given LSD-associated enzyme in the ER, enabling trafficking to the lysosome, are undergoing clinical evaluation17. The focus of this paper is to demonstrate that it is possible to ameliorate LSDs by utilizing small molecule proteostasis regulators that adapt the proteostasis network through a post-translational mechanism, as opposed to the transcriptional and translational approach employed previously13.

Gaucher's disease, the most prevalent LSD, is caused by deficient lysosomal glucocerebrosidase (GC) activity16,17,21,22. This results in the accumulation of glucosylceramide, the GC substrate, in the lysosomes of several cell types, leading to hepatomegaly, splenomegaly, anemia, thrombocytopenia, and in severe cases, central nervous system involvement21. The GC enzyme is an N-linked glycoprotein that has to fold in the ER to engage its trafficking receptor, enabling trafficking through the Golgi and on to the lysosome. The most common GD-associated GC mutations are N370S and L444P25, both being misfolding- and ERAD-prone, the latter associated with neuropathic GD.

We previously proposed that compounds that inhibit L-type voltage-gated Ca^{2+} channels would minimize depletion of the ER Ca^{2+} store by reducing Ca^{2+}-induced Ca^{2+} release, thought to be important in minimizing GD pathology12 because glucosylceramide accumulation in GD deleteriously enhances agonist-induced calcium release from ER stores via the ryanodine receptors (RyRs)16,26-28. Herein we show that elevating ER Ca^{2+} levels (by overexpressing the SERCA2b Ca^{2+} influx pump or by inhibiting the RyR ER Ca^{2+} efflux channels) enhances the folding, trafficking and function of N370S and L444P GC in GD-derived fibroblasts. Small molecule proteostasis regulators that increase the ER Ca^{2+} concentration appear to enhance the capacity of calnexin to fold mutant misfolding-prone enzymes in the ER by resculpting their folding free energy diagrams, increasing the mutant GC population that can engage the trafficking receptor at the expense of ER-associated degradation. These small molecules post-translationally regulate calnexin's function, and unlike unfolded protein response activators, this category of proteostasis regulators does not induce transcription of stress-responsive genes.

Results

RyR(s) siRNA treatment enhances L444P GC proteostasis

Diltiazem **1** or verapamil **2**, besides inhibiting plasma membrane L-type Ca^{2+} channels to antagonize RyR–mediated calcium-induced ER calcium release12, can also directly inhibit

Author Manuscript Author Manuscript Author Manuscript Author Manuscript

ER Ca^{2+} efflux by targeting the RyRs29,30 (Fig. 1a. See Supplementary Fig. 1 for the structures of all compounds used in this paper). Since not all L-type Ca^{2+} channel antagonists function as GC proteostasis regulators12, we tested the hypothesis that direct antagonism of RyR ER Ca^{2+} efflux channels by diltiazem **1** and verapamil **2** in patient-derived homozygous L444P GC fibroblasts (L444P fibroblasts hereafter) explains the enhanced L444P GC folding, trafficking and function (proteostasis). Enhancing L444P GC proteostasis is very challenging because of this variant's prominent ER misfolding and ERAD (see below)25. L444P fibroblasts express two of the three RyR isoforms31, isoforms 2 and 3, with the latter being prominent (Supplementary Fig. 2a). RyR3 siRNA knockdown led to a 50-70% reduction in the RyR3 transcript based on RT-PCR. We were not able to reliably quantify the RyR2 siRNA knockdown, due to low transcript levels.

Decreasing transcription of individual RyRs by siRNA treatment partially restored L444P GC enzyme activity, increasing it by 1.2 fold (RyR1), 1.4 fold (RyR2) and 1.5 fold (RyR3) (*, $p<0.01$; **, $p<0.001$), as assessed by the intact fibroblast assay (Fig. 1b and Supplementary Fig. 2b)17. Co-application of siRNAs to RyR3 and another RyR isoform further increased L444P GC enzyme activity (RyR1 and RyR3: 1.6 fold; RyR2 and RyR3: 1.8 fold) (Fig. 1b and Supplementary Fig. 2b), nearly doubling cellular L444P GC enzyme activity from 12.5 to 25% of WT levels–an increase that is expected to ameliorate GD21. Reducing ER Ca^{2+} efflux by siRNA targeting the RyR(s) is comparable to the rescue achieved by diltiazem, which inhibits both L-type Ca^{2+} channels and the RyRs12 (Fig. 1b, black bar, and see below), suggesting that RyR inhibition is sufficient to explain the activity of diltiazem **1** or verapamil **2**.

To determine whether the increased GC enzyme activity is due to enhanced L444P ER folding and trafficking in the siRNA-treated fibroblasts, cell lysates were treated with endoglycosidase H (endo H) and then analyzed by Western blot. Endo H cleaves after Asn-GlcNAc in the N-linked glycan installed on GC in the ER, but cannot remove this oligosaccharide chain after the high mannose form is enzymatically remodeled in the Golgi. Because mutant GC has to fold in the ER to engage its receptor for vesicular transport to the Golgi, an increase in the endo H resistant band is a surrogate for reporting on increased folding efficiency of GC in the ER (although it does not directly demonstrate this) and trafficking at least to the Golgi. The lower molecular weight band corresponding to endo H sensitive GC that has not left the ER is typically detected as a prominent band after endo H treatment of lysates from cells harboring a misfolding-prone GC (e.g., L444P GC) (Fig. 1c, lane 2)20,23. The siRNA-mediated knockdown of individual RyRs resulted in a detectable increase in the endo H resistant (post-ER) GC glycoform (upper band in Fig. 1c, cf. lanes 4 and 2 for RyR1, lanes 6 and 2 for RyR2, and lanes 8 and 2 for RyR3; quantification shown by black bars directly below; also see Supplementary Fig. 2c), consistent with increased ER folding efficiency required for Golgi trafficking. Co-application of siRNA against RyR3 and RyR2 or RyR3 and RyR1 further increased the endo H resistant GC glycoform intensity (Fig. 1c, cf. lane 12 to lanes 10 and 16 for RyR3 and RyR1, lane 14 to lanes 10 and 16 for RyR3 and RyR2; quantification shown by black bars directly below).

Indirect immunofluorescence microscopy was employed to detect the total amount of L444P GC produced and whether L444P GC is trafficked to the lysosome upon RyR(s)

Author Manuscript Author Manuscript Author Manuscript Author Manuscript

knockdown. L444P GC is barely detectable in fibroblasts due to extensive ERAD20 (Fig. 1d, top row, GC in green, the LAMP2 lysosomal marker in red, overlap artificially colored white). Lysosomal colocalization is discernable after the application of siRNA against RyR3 (Fig. 1d, middle row) and increasingly apparent after the co-application of siRNA against RyR3 and RyR2 (Fig. 1d, bottom row).

Inhibitors of the RyR(s) enhance mutant GC proteostasis

We next explored whether pharmacologic inhibition of the RyRs (Fig. 1a) could also enhance GC proteostasis. Diltiazem **1** and two RyR antagonists, namely dantrolene **3** (a very selective RyR antagonist) and DHBP **4** 32,33 (Fig. 2a), were administered to L444P fibroblasts for 5 d before cell lysis, endo H digestion and western blot analysis was performed. Diltiazem **1** or dantrolene **3** (10 and 25 μM) or DHBP **4** (3 μM) treatments significantly increased the endo H resistant GC bands (Fig. 2a, cf. lanes 6 and 4 to lane 2 for diltiazem **1**, cf. lanes 12 and 10 to lane 8 for dantrolene **3**, and cf. lane 16 to lane 14 for DHBP **4**; quantification shown by black bars directly below), indicating that RyR inhibitors enhance mutant L444P GC ER folding and trafficking. DHBP utilized at 3 μM led to ≈ 10 % cell death after 4 d, an effect that was exacerbated at higher concentrations (Supplementary Fig. 3). The increase in the L444P endo H resistant GC bands after diltiazem **1**12 or dantrolene **3** treatment was not due to increased GC mRNA levels (Supplementary Fig. 4).

The lysed cell GC activity assay revealed significantly ($p<0.001$) increased L444P GC activity after a 7 d treatment of L444P fibroblasts with diltiazem **1** (10 μM, 1.9 fold), verapamil **2** (3 μM, 1.5 fold), dantrolene **3** (25 μM, 1.3 fold), and DHBP **4** (3 μM, 1.4 fold) (Fig. 2b). Indirect immunofluorescence microscopy revealed that L444P GC lysosomal colocalization (white) becomes more apparent after dantrolene **3** (25 μM) treatment for 10 d (Fig. 2c, cf. lower and upper (vehicle control) far right panels). Dantrolene **3** (10 μM) significantly increased GC activity (intact cell GC activity assay) in patient-derived homozygous N370S GC fibroblasts (1.7 fold) and WT fibroblasts (1.3 fold, $p<0.001$) (Fig. 2d), similar to the 2-fold increase (along with trafficking increases) observed previously12 in diltiazem **1**-treated N370S GC fibroblasts (Supplementary Fig. 5), implying that inhibition of the RyRs (and possibly L-type Ca^{2+} channels for diltiazem **1**) enhance WT and N370S GC proteostasis. The intact cell assay revealed that dantrolene **3** slightly decreased L444P GC activity (Supplementary Fig. 6a), in striking contrast to the lysed cell assay (Fig. 2b).

Since L444P GC is hypersensitive to inhibition, the difference in the L444P GC enzyme activity of dantrolene-treated fibroblasts assessed using the lysed cell assay (Fig. 2b; employing a 10-fold dilution)17 versus the intact cell assay (Supplementary Fig. 6a) may be due to L444P GC inhibition. Thus, binding to the active site and inhibition of WT GC *in vitro* was assessed next. Cerezyme, a recombinant version of WT GC, was incubated with verapamil **2** (0.01 to 1000 μM), dantrolene **3** (0.3 to 300 μM) or DHBP **4** (0.3 to 400 μM), before GC enzyme activity was assayed (Supplementary Fig. 6b). The data for diltiazem **1** and NN-DNJ **5** (known GC inhibitor) have been reported previously12 and are included to facilitate a comparison. Diltiazem **1**, verapamil **2**, and DHBP **4** do not inhibit WT GC in this

Author Manuscript Author Manuscript Author Manuscript Author Manuscript

concentration range, whereas dantrolene **3** exhibits a half maximal inhibitory concentration (IC_{50}) of ~ 90 μM toward Cerezyme (Supplementary Fig. 6b), suggesting that the cell culture media concentration of dantrolene (25 μM) used in our experiment could inhibit L444P GC. To evaluate this possibility, we co-applied dantrolene **3** and MG-132 **6** (GC proteostasis regulator that activates the unfolded protein response13) to L444P fibroblasts, reasoning that if dantrolene were a L444P GC inhibitor, it would inhibit the increased amount of folded and trafficked L444P GC resulting from MG-132 **6** treatment, resulting in lower L444P GC activity. Indeed, administering dantrolene **3** (10 μM) and MG-132 **6** (0.25 μM) to fibroblasts for 4 d afforded a 2.4 fold increase in L444P GC enzyme activity, which is lower than the 3.7 fold increase observed with MG-132 **6** alone (Supplementary Fig. 6c), suggesting that dantrolene **3** can inhibit the increased L444P GC lysosomal pool in the intact cell assay.

Five IP_3R Ca^{2+}-efflux channel (Fig. 1a) antagonists **7-11**34 (see Supplementary Fig. 1 for structures) were also evaluated for their effect on GC activity in L444P fibroblasts. IP_3 receptor antagonists did not increase L444P GC activity after a 7 d treatment period in the intact cell assay (Supplementary Fig. 7a). siRNA knockdown of IP_3R isoforms 2 and 3 (expressed in L444P fibroblasts (Supplementary Fig. 7b)) either alone, or in combination, did not significantly change the L444P GC enzyme activity in the intact cell assay either (Supplementary Fig. 7d) in spite of efficient knockdown (Supplementary Fig. 7c), suggesting that ER Ca^{2+} levels with IP_3R antagonism are not high enough to influence GC proteostasis (a hypothesis supported by the ER Ca^{2+} concentration measurements discussed below upon IP_3R antagonist treatment).

Overexpressing SERCA2b enhances L444P GC proteostasis

To further support the hypothesis that elevated ER Ca^{2+} levels enhance mutant GC proteostasis, we overexpressed the sarco/ER Ca^{2+} influx ATPase pump isoform 2b (SERCA2b) (Fig. 1a) in L444P GC and N370S GC fibroblasts. SERCA2b is the most widespread of all the SERCA isoforms, playing a critical role in clearing cytosolic Ca^{2+} and maintaining ER Ca^{2+} concentrations35. When SERCA2b was transiently overexpressed (quantification in Fig 3a, far right, orange bars), the L444P GC post-ER glycoform band increased significantly in comparison to the empty vector control (Fig. 3a; cf. lane 4 to lane 2, see black bars on the right (and inset) for quantification) and L444P GC activity increased 1.5 fold (**, $p<0.001$, intact cell assay, Fig. 3b, left panel). Analogous SERCA2b overexpression in N370S GC fibroblasts increased activity 1.3 fold (**, $p<0.001$, intact cell assay, Fig. 3b, right panel), and increased the post-ER glycoform band (Fig. 3c; cf. lane 4 to lane 2, see black bars on the right (and inset) for quantification). Treatment with thapsigargin **12**, a very potent SERCA inhibitor, decreased L444P GC activity by 30 % over 7 d (Fig. 3d, left, intact cell assay), demonstrating the importance of SERCA in maintaining sufficient ER Ca^{2+} levels for GC proteostasis. Curcumin **13**, a less potent SERCA2 inhibitor, had less of an effect on L444P GC enzyme activity (Fig. 3d, right).

Acute and chronic RyR antagonism increases ER Ca^{2+} levels

The genetically encoded ER Ca^{2+} sensor, D1-ER cameleon36, was used to measure relative ER Ca^{2+} concentration ($[Ca^{2+}]_{ER}$) changes in response to RyR antagonist treatments.

Author Manuscript Author Manuscript Author Manuscript Author Manuscript

Patient-derived L444P fibroblasts were imaged 2-3 days after transfection with D1-ER cameleon. Treatment of these fibroblasts with diltiazem **1** (50 μM) or DHBP **4** (50 μM) significantly increased the YFP to CFP fluorescence ratio over a time course of 400 s, indicating acute $[Ca^{2+}]_{ER}$ increases (Fig. 4a). In contrast, there was no measurable acute change in $[Ca^{2+}]_{ER}$ after treatment with IP_3R antagonists Xestospongin C **7** (50 nM) and thimerosal **10** (10 μM) (data not shown), consistent with our finding that they do not enhance mutant GC proteostasis (Supplementary Fig. 7). Unfortunately, the fluorescence of dantrolene **3** overlaps with the D1-ER cameleon FRET signal, rendering its acute $[Ca^{2+}]_{ER}$ measurements unreliable. Transfection with D1-ER cameleon slightly alters the morphology of the ER in L444P fibroblasts, thus we felt that it was more appropriate to use HeLa cells for longer term $[Ca^{2+}]_{ER}$ measurements, as the ER of HeLa remains unaltered after D1-ER cameleon transfection. Moreover, HeLa cells and L444P fibroblasts display similar RyR isoform distributions (Supplementary Fig. 8a). In addition, diltiazem **1** (50 μM) treatment of HeLa cells previously transfected with DI-ER cameleon confirmed the acute increase in $[Ca^{2+}]_{ER}$ (Supplementary Fig. 8b).

HeLa cells were transfected with D1-ER cameleon and after 1 day they were treated with diltiazem **1** (25 μM) or dantrolene **3** (25 μM) for another 2 d before being subjected to ER Ca^{2+} imaging (Fig. 4b) to discern whether the steady-state $[Ca^{2+}]_{ER}$ remains elevated upon long term drug treatment. In this experiment the cells are washed before they are imaged to remove the drug, allowing dantrolene **3** to be used. Application of thapsigargin **12** (5 μM) along with ionomycin **15** (5 μM) and EGTA **16** (7.5 mM) depletes Ca^{2+} from the ER enabling a comparison of drug-treated steady-state ER Ca^{2+} levels with the depleted ER Ca^{2+} levels. Treatment of HeLa cells with diltiazem **1** (25 μM) or dantrolene **3** (25 μM) for 2 d leads to significantly elevated steady-state $[Ca^{2+}]_{ER}$ compared to the untreated control sample, as represented by a higher steady-state YFP/CFP emission ratio, while not altering the depleted $[Ca^{2+}]_{ER}$ significantly (Fig. 4b). The steady-state YFP/CFP ratios (mean ± SEM, n = 12) were 2.48 ± 0.05, 2.72 ± 0.04, and 2.78 ± 0.05 for the untreated control sample, the diltiazem **1** treated sample, and the dantrolene **3** treated sample, respectively, while the depleted ER Ca^{2+} state YFP/CFP ratios (mean ± SEM, n = 12) were 1.71 ± 0.05, 1.78 ± 0.05, and 1.80 ± 0.05, respectively.

To complement these measurements using patient-derived fibroblasts, the steady-state cytosolic Ca^{2+} concentrations of L444P fibroblasts were shown to decrease after treatment with diltiazem **1** (25 μM) for 24 and 96 h as demonstrated by a decrease of the Fura2 fluorescence ratio (340/380) (Fig. 4c), consistent with the observed increase in $[Ca^{2+}]_{ER}$ in fibroblasts and HeLa cells noted above. That the RyR antagonists increased $[Ca^{2+}]_{ER}$ and enhanced mutant GC proteostasis, while thapsigargin **12** decreased $[Ca^{2+}]_{ER}$ and reduced mutant GC proteostasis strongly indicates that the $[Ca^{2+}]_{ER}$ influences mutant GC proteostasis. Consistent with this hypothesis, IP_3R antagonism does not affect $[Ca^{2+}]_{ER}$ or GC proteostasis.

RyR antagonism does not activate the stress responses

The established GC proteostasis regulators celastrol **14** and MG-132 **6** activate both the heat shock response (HSR) and the unfolded protein response (UPR), the UPR being functionally

Author Manuscript Author Manuscript Author Manuscript Author Manuscript

important13. Thus, we probed whether diltiazem **1** (10 μM) or dantrolene **3** (10 and 25 μM) induced the UPR or HSR in L444P fibroblasts,6-9,13 after 1, 3, 5, 7 and 10 d of treatment (see dosing schedule in Supplementary Fig. 9a). DHBP **4** exhibits cytotoxicity which could result in a UPR or HSR and was not analyzed. The relative mRNA levels of cytoplasmic HSR-associated chaperones (Hsp40, 70, 90, 27) did not change significantly after diltiazem **1** (published previously12) or dantrolene **3** treatment (Supplementary Fig. 9a). Western blot analysis of key cytoplasmic HSR-transcriptional program regulated chaperones confirmed the absence of a HSR upon diltiazem **1** (published previously12) or dantrolene **3** (Fig. 4d) treatments. Similarly, diltiazem **1** or dantrolene **3** treatment failed to induce the UPR. There was no significant increase in the expression levels of CHOP (a reporter of the PERK arm of the UPR9) or spliced XBP1 (a reporter of the IRE1 arm of the UPR9) (Fig. 4e and Supplementary Fig. 9b). Western blot analysis of chaperones and enzymes under control of the UPR further confirms the inability of these agents to activate classical stress-responsive signaling pathways (Fig. 4d).

Calnexin overexpression enhances L444P GC proteostasis

We next tested the hypothesis that increased ER Ca^{2+} levels promote the folding of mutant GC by upregulating the activity of Ca^{2+}-regulated ER chaperones such as calnexin, calreticulin or BiP/GRP78 37-39. Transient overexpression of calnexin in L444P fibroblasts (Fig. 5a; quantification far right, orange bars) increased the endo H resistant band (Fig. 5a; cf. lane 4 to lane 2, see black bars far right and inset for quantification) and significantly increased (**, $p<0.001$) L444P GC activity (~ 1.6 fold) (Fig. 5b, blue bars, intact cell assay). Calnexin overexpression also increased N370S GC enzyme activity (~ 1.4 fold; *, $p<0.01$) (Fig. 5b, red bars; calnexin quantification, far right, orange bars).

The siRNA-mediated knockdown of calnexin (Supplementary Fig. 10; ~ 50 % efficiency; orange bars, far right) did not measurably alter the endo H sensitive or endo H resistant L444P GC levels in L444P fibroblasts, but did result in a statistically significant decrease in L444P GC activity (~17 %; **, $p<0.001$), relative to the non-targeting siRNA control (Fig. 5c, intact cell assay), suggesting that calreticulin can only partially functionally substitute. Consistent with this hypothesis, the knockdown of calreticulin resulted in a similar decrease in the total L444P GC protein and activity (Supplementary Fig. 11a and 11b). The overexpression of calreticulin, however, did not significantly affect total L444P protein level or activity (Supplementary Fig. 11c and 11d).

Transient overexpression of BiP in L444P fibroblasts did not alter total GC levels or activity (Supplementary Fig. 12), suggesting that if BiP is involved in GC proteostasis, is not limiting. Since calnexin forms a complex with the ER oxidoreductase ERp57, which could catalyze the formation of GC's native disulfide bond40, we also examined the effect of ERp57 RNAi treatment on the L444P proteostasis. There was no significant change in the endo H resistant glycoform or L444P GC activity after siRNA knockdown (Supplementary Fig. 13), suggesting that if ERp57 is involved in GC proteostasis, its levels after RNAi treatment were not limiting.

Author Manuscript Author Manuscript Author Manuscript Author Manuscript

The calnexin-GC protein interaction is Ca^{2+}-dependent

We next explored whether calnexin was chaperoning GC folding and whether this interaction was Ca^{2+}-dependent. Genes encoding WT, L444P and N370S GC proteins fused to a VSVG C-terminal tag (enabling efficient immunoprecipitation using a mouse monoclonal anti-VSVG antibody) were constructed. The expression levels of these constructs when overexpressed in HeLa cells were compared using the same amount of plasmid DNA for each transfection. While overexpressed L444P GC is barely observable (Fig. 6a, row 1, lane 5), as in human L444P GD fibroblasts (due to ER misfolding and ERAD20), WT GC and N370S GC proteins appear to be prominently expressed, as in human GD fibroblasts (Fig. 6a, row 1, lanes 3 and 7).

If proper GC folding were dependent on calnexin, overexpression of calnexin should enhance mutant GC proteostasis. Thus, WT, L444P and N370S GC proteins were overexpressed (using equal amounts of plasmid DNA as above) along with calnexin in HeLa cells by transient transfection. Western blot analysis of the HeLa lysates revealed that WT, L444P and N370S GC levels were significantly higher with calnexin overexpression (Fig. 6a, row 1 cf. lanes 3 to 4, 5 to 6, and 7 to 8), despite only modest overexpression of calnexin (Fig. 6a, row 2, cf. lanes 3 to 4, 5 to 6, and 7 to 8). Since calnexin could be influencing GC proteostasis by direct binding of partially folded states or indirectly, e.g., by upregulating GC proteostasis components or a native state binding protein, the GC protein and its bound partners were immunoprecipitated from the HeLa lysate using the anti-VSVG antibody. There is much more calnexin bound to the GC variants when calnexin is overexpressed (Fig. 6a, row 2, cf. lanes 11 to 12, 13 to 14, 15 to 16), suggesting that the increased total GC levels were a result of more calnexin being available to chaperone mutant GC folding, presumably by resculpting the mutant GC folding free energy diagram.

We next probed whether the calnexin-GC interaction is Ca^{2+}-dependent. A cell lysate prepared from HeLa cells overexpressing the GC proteins of interest, but not overexpressing calnexin, was treated with EGTA, a specific Ca^{2+} ion chelator, prior to VSVG antibody-mediated immunoprecipitation. Pre-incubation of the lysate with EGTA led to an obvious decline in calnexin in complex with the GC protein (Fig. 6b, row 2, cf. lanes 7 to 8, 9 to 10 and lanes 11 to 12). Dividing the calnexin band intensity by the GC band intensity derived from western blot densitometry measurements clearly shows that the interaction between these two proteins is significantly reduced in the presence of EGTA (Fig. 6c). This provides strong evidence that the calnexin-GC protein interaction is Ca^{2+} regulated, partially explaining why ER Ca^{2+} ion concentration increases enhance mutant GC proteostasis.

Enhancing calnexin's ER Ca^{2+} regulated chaperoning of GC

We next explored whether dantrolene **3** treatment enhanced the Ca^{2+}-dependent interaction between calnexin and GC. Calnexin and its associated proteins was immunoprecipitated, using a rabbit polyclonal anti-calnexin antibody, from a cell lysate prepared from L444P fibroblasts treated with dantrolene **3** or DMSO (vehicle control). The amount of L444P GC protein bound to calnexin was assessed by western blot analysis. Dantrolene **3** treatment significantly increased the amount of L444P GC protein that is bound to calnexin (Fig. 6d, row 1, cf. lanes 5 to 6) without increasing the pool of calnexin present (Fig. 6d, row 2, cf.

Author Manuscript Author Manuscript Author Manuscript Author Manuscript

lanes 5 to 6). The GC-calnexin interaction was specific, since an irrelevant antibody (anti-VSVG antibody) failed to pull down either GC (Fig. 6d, row 1, lanes 3 and 4), or calnexin (Fig. 6d, row 2, lanes 3 and 4). Similarly, more L444P GC protein was bound to calnexin in L444P fibroblasts treated with diltiazem **1** (Fig. 6e, row 1, cf. lanes 5 to 6), with no change in the calnexin level in the treated fibroblasts (Fig. 6e, row 2, cf. lanes 5 to 6).

To further demonstrate that dantrolene **3** treatment enhances the Ca^{2+}-dependent calnexin-GC protein interaction, we pre-incubated cell lysate prepared from L444P fibroblasts treated with dantrolene **3** or DMSO with EDTA (a general metal chelator) or EGTA (a Ca^{2+}-specific chelator), prior to immunoprecipitation with the anti-calnexin antibody. In the presence of EDTA or EGTA, the dantrolene **3**-mediated increase in L444P GC protein that interacted with calnexin was significantly reduced (Fig. 6f, row 1, cf. lanes 5 to 6, 11 to 12).

Discussion

The ryanodine receptor antagonist category of proteostasis regulators increases ER Ca^{2+} levels and post-translationally regulates the folding capacity of the calnexin (and possibly calreticulin), presumably enhancing mutant GC ER folding (although this cannot be shown directly), thus enabling increased mutant GC trafficking to and function within the lysosome. Genetic strategies that increase ER Ca^{2+} levels function analogously. Increased ER Ca^{2+} levels increase the affinity of the calnexin•mutant GC interaction, seemingly explaining the enhancement in mutant GC ER folding at the expense of ERAD by binding to GC folding intermediates and resculpting the folding free energy diagram to increase the concentration of mutant GC that traffics to the lysosome. Consistent with this mechanistic proposal, the association of calnexin with other client proteins, including the MHC class I heavy chain41, the α-subunit of the nicotinic acetylcholine receptor42 and apolipoprotein(a)43, was found to enhance folding efficiency at the expense of ERAD. However, our data does not exclude the possibility that ER Ca^{2+} increases could activate or repress Ca^{2+} signaling pathways that influence GC proteostasis by additional mechanisms.

Calnexin (and calreticulin) is known to bind to glycoproteins through a lectin site with specificity for $Glc_1Man_9GlcNAc_2$ and/or through a polypeptide binding site that recognizes exposed hydrophobic surfaces in folding intermediates44. Biochemical44 and X ray crystallographic38 studies identify a single, ER-lumenal, low affinity Ca^{2+} binding site (K_d ~ 0.15 ± 0.05 mM) on the N-terminal β-sandwich of calnexin that may serve a structural role. Occupancy of this Ca^{2+} binding site enhances calnexin's binding to the oligosaccharide substructure of N-linked glycoproteins45 and its ability to suppress the aggregation of non-glycosylated firefly luciferase44, rationalizing why ER Ca^{2+} increases appear to increase the affinity or specificity of the interaction between calnexin and partially folded GC mutants. There is another putative moderate affinity Ca^{2+} binding site within the C-terminal domain of calnexin46, but its cytoplasmic localization suggests that it is unlikely to influence the calnexin•GC interaction. Calreticulin's function seems to be regulated analogously, as there is a putative Ca^{2+} binding site on its ER lumenal N-domain47.

The basis for why the increased ER Ca^{2+} concentration-mediated post-translational regulation of the calnexin folding pathway can increase mutant GC proteostasis, while not

Author Manuscript Author Manuscript Author Manuscript Author Manuscript

permitting the secretion of unfoldable proteins or increasing the steady state levels of many other secreted proteins is emerging. Unpublished mass spectrometry data (Wang, Mu, Yates and Kelly) reveal that the folding and trafficking efficiency, reflected by steady state levels of secreted proteins, is largely unchanged upon diltiazem treatment. Strictly analogous data demonstrate that there was a modest change (~10%) in the steady state levels of a small subset of secreted proteins upon activation of the UPR13. The selectivity of proteostasis regulators for mutant misfolding-prone proteins is rationalized on the basis of the "minimum export threshold" hypothesis48, in which it is hypothesized that the vast majority of the secreted proteome exhibits sufficiently rapid folding kinetics and slow unfolding/misfolding/aggregation kinetics that the basal proteostasis network capacity is sufficient to very efficiently fold these proteins. Thus, enhancing the proteostasis network capacity will not increase the folding and trafficking efficiency or the steady state concentration of these proteins—an example of the first level of selectivity of this class of proteostasis regulators. But for mutant disease-associated proteins that exhibit compromised folding energetics, increasing the capacity of the calnexin folding pathway has a profound influence on the efficiency of folding.

The ryanodine receptor antagonist category of proteostasis regulators do not rescue disease-associated proteins that are not critically dependent on the calnexin folding pathway, e.g., ΔF508 CFTR mutant that causes Cystic Fibrosis (Balch, W.E., personal communication), demonstrating a second level of selectivity. Proteostasis regulators that function by post-translational regulation of the calnexin folding pathway or by transcriptional UPR activation do not increase the secretion of proteins that cannot fold under any conditions, because these proteins cannot engage their trafficking receptors, demonstrating a third level of selectivity. Instead, the unfoldable proteins engage the ERAD pathway leading to their efficient proteosomal degradation.

The ryanodine receptor antagonist proteostasis regulators should be sufficient to ameliorate GD, as the mutant GC lysosomal enzyme activity achieved in fibroblasts exceeds 10 % WT activity, thought to be the approximate disease threshold. We envision that the increased Ca^{2+}-mediated calnexin binding to partially folded mutant GC affords more trafficking-competent folded GC in the ER by resculpting the folding free energy diagram of mutant GC—maximizing the folded mutant GC concentration while minimizing aggregation and misfolding. Since one third of the human proteome is N-glycosylated and utilizes the ER for folding and the secretory pathway to achieve function, the strategy outlined within could become generally useful for enhancing the folding efficiency of mutant misfolding-prone N-linked glycoproteins that are dependent on calnexin or calreticulin and whose misfolding leads to loss-of-function diseases, such as the > 50 lysosomal storage diseases.

Methods

Enzyme activity assays

The differences between and the applicability of the intact cell and the lysed cell GC activity assay are described in the Supplementary Methods section. Briefly, the intact cell assay allows an assessment of what is likely to happen in a patient when a given pharmacologic or genetic manipulation is used and therefore has the potential to identify promising GD

Author Manuscript Author Manuscript Author Manuscript Author Manuscript

therapies. The lysed cell activity assay is employed whenever slight cell toxicity is detected with a given compound because it prevents underestimation of GC enzyme activity due to variation in cell numbers after drug treatment. The lysed cell assay allows identification of compounds that increase enzyme concentration (through enhancement of folding and trafficking) while also inhibiting the enzymes.

Western blot analysis

Cells were lysed with complete lysis-M buffer containing Roche complete protease inhibitor cocktail. Company specifications (New England Biolabs) were followed for endo H treatment. Aliquots of cell lysates were separated using a 10 % SDS-PAGE gel and visualized by western blot analysis using appropriate antibodies (see Supplementary Methods for details). Bands in endo H treated samples were quantified using NIH Image J software.

Indirect immunofluorescence microscopy

As described previously 23, cells grown on glass cover slips were fixed with 3.7% paraformaldehyde in PBS for 15 min. The cover slips were washed with PBS, quenched with 15 mM glycine in PBS for 10 min, and then the cells permeabilized with 0.2 % saponin in PBS for 15 min. Cells were incubated for 1 h with primary antibodies (diluted 1:1,000 for the mouse monoclonal anti-GC 8E4, and diluted 1:10,000 for the rabbit anti-LAMP2), washed with 5 % goat serum in PBS, and incubated for 1 h with secondary antibodies (Alexa Fluor 488 goat anti-mouse IgG and Alexa Fluor 546 goat anti-rabbit IgG from Molecular Probes). Images were collected using a Bio-Rad (Zeiss) Radiance 2100 Rainbow laser scanning confocal microscope attached to a Nikon TE2000-U microscope, and analyzed using NIH Image J software. The experiments were repeated three times with similar results.

ER Ca^{2+} Imaging

The genetically encoded Ca^{2+} indicator, D1-ER cameleon, was used to measure ER Ca^{2+} levels, as previously described36. Briefly, L444P fibroblasts and HeLa cells were plated on 35-mm glass-bottomed dishes and transfected the next day with 1 μg of D1-ER cameleon using Fugene 6. The cells were washed with Hanks balanced salt solution containing 20 mM HEPES (pH 7.4) 2-3 days after transfection, and imaged using a Zeiss Axiovert 200M microscope with a Cascade 512B cooled charge-coupled device camera, controlled by METAFLUOR 6.1 software. Emission ratio imaging of the ER cameleon was accomplished using a 430/24 excitation filter, 450-nm dichroic mirror, and two emission filters (470/24 for CFP and 535/20 for YFP) controlled by a Lambda 10-3 filter changer. The background corrected fluorescence ratio of YFP/CFP (upon CFP excitation) is a measure of relative ER Ca^{2+} levels. The details of the acute versus chronic ER Ca^{2+} concentration measurements can be found in the Supplementary Methods.

Intracellular Ca^{2+} measurement

Fura-2, AM (Invitrogen #F1225) was used to measure intracellular Ca^{2+} levels according to company specifications. Briefly, approximately 1×10^4 L444P fibroblasts were plated per

Author Manuscript Author Manuscript Author Manuscript Author Manuscript

well in 96-well plates (100 μl per well) overnight to allow cell attachment. The cells were washed twice with Hanks balanced salt solution (HBSS), incubated with 5 μM Fura-2, AM plus 0.05% Pluronic F-127 (Invitrogen #P3000MP) at RT for 30 min, washed twice with HBSS, and maintained at RT for another 15 min. Fluorescence was measured by using excitation at 340 nm and 380 nm and emission at 510 nm with a SpectraMax Gemini fluorescence plate reader. The background corrected fluorescence ratio of Fura-2 (340/380) is a measure of relative intracellular Ca^{2+} levels. Each data point was evaluated in at least sixteen replicates, and on three different days. Data are reported as mean ± SEM.

Quantitative RT-PCR

The relative mRNA expression levels of target genes were measured using quantitative RT-PCR after treating the L444P fibroblasts with dantrolene or diltiazem12,13. The protocol is detailed in the Supplementary Methods, primers used are listed in Supplementary Table S1.

siRNA transfection

L444P fibroblasts were seeded at approximately 2×10^5 cells per well in 6-well plates and allowed to reach ~80% confluency before transfection. The small interfering RNA (siRNA) duplexes from Dharmacon were: ON-TARGETplus Duplex RyR1 (J-006292-05-0010), RyR2 (J-006293-05-0010), RyR3 (J-006294-05-0010 or L-006294-00-010 for SmartPool), CANX (J-003636-07-0005), CALR (J-008197-06-0005), PDIA3 (J-003674-09-0005), ITPR2 (J-006208-05-0005), ITPR3 (J-006209-06-0005) and Non-Targeting siRNA (D-001810-01-20) as control. Cells were transfected with 50 nM siRNA using HiPerfect Transfection Reagent (Qiagen) according to the manufacturer's transfection protocol. The protein, RNA and intact cell GC activity were analyzed after the indicated siRNA dosing schedule.

Plasmids and transfection

The pcDNA3.1+WT GC-VSVG plasmid was produced by ligating the WT GC cDNA (amplified from a plasmid that harbors the WT GC cDNA (kindly provided by Professor Ernest Beutler, TSRI) using the following primers (5′ to 3′): GTTGCTAGCGGGATGGAGTTTTCAAGTCCTTCC and GTTACCGGTCTGGCGACGCCACAG) into the pcDNA3.1+VSVG plasmid (kindly provided by Professor W.E. Balch, TSRI). This plasmid enables the overexpression of the WT GC with a short VSVG tag (YTDIEMNRLGK) at the C-terminus. The pcDNA3.1+L444P GC-VSVG and pcDNA3.1+N370S GC-VSVG plasmids were generated using Quikchange II site-directed mutagenesis (Stratagene) as specified by the manufacturer, using the following primers (5′ to 3′): CAGTCAGAAGAACGACCCGGACGCAGTGGCACTG and CAGTGCCACTGCGTCCGGGTCGTTCTTCTGACTG for L444P, CCACAGCATCATCACGAGCCTCCTGTACCATGTGG and CCACATGGTACAGGAGGCTCGTGATGATGCTGTGG for N370S. The proper construction of all plasmids was confirmed by DNA sequencing. HeLa cells, L444P and N370S fibroblasts were seeded at approximately 2×10^5 cells per well in 6-well plates or 10^4 cells per well in 96-well plates for protein analysis and intact cell GC activity assay, respectively. Cells were allowed to reach ~80% confluency before transient transfection

Author Manuscript Author Manuscript Author Manuscript Author Manuscript

using Lipofectamine 2000 transfection reagent (Invitrogen) or Fugene 6 transfection reagent (Roche), according to the manufacturers' instructions. Transfection of N370S fibroblasts using Fugene 6 leads to slight cytotoxicity. After the indicated incubation times, the cells were harvested for the corresponding analyses.

Immunoprecipitation

Cells were lysed with lysis buffer (50 mM Tris, pH 7.5, 150 mM NaCl, 1 % Triton X-100) supplemented with complete protease inhibitor cocktail. The mouse monoclonal anti-VSVG antibody (kindly provided by Professor W.E. Balch, TSRI) or rabbit polyclonal anti-calnexin antibody (Stressgen) was added to the cell lysate and incubated overnight at 4 °C. After the addition of 30 μl of GammaBind G sepharose bead slurry (~50% v/v in lysis buffer, GE Healthcare), the resulting mixture was placed on a rocker for 2 h at 4 °C. Non-specifically bound proteins were removed from the beads by washing three times with lysis buffer. Bound proteins were eluted by boiling the beads in SDS loading buffer in the presence of DTT. The effect of calcium on the calnexin-GC protein interaction was performed as described previously49. Briefly, the lysate was incubated with 2 mM EDTA or EGTA for 15 min at 37 °C prior to the addition of the indicated antibody for immunoprecipitation.

Statistical analysis

All data are presented as mean ± SEM or mean ± SD as stated and any statistical significance was calculated using a two-tailed Student's t-Test.

Supplementary Material

Refer to Web version on PubMed Central for supplementary material.

Acknowledgments

We thank Professor W.E. Balch (TSRI), Professor Michael Brenner (Harvard Medical School), Dr. Kim Green (University of California, Irvine) and Professor Tohru Mizushima (Kumamoto University) for their generosity in providing us with the Ap^r-M8-CNX50, SERCA2 cDNA, pCR(HA) and pcDNA3.1−GRP78 plasmids, respectively, Dr. Hans Aerts (University of Amsterdam, Netherland) for the mouse monoclonal anti-GC 8E4, Dr. Michiko Fukuda for the rabbit anti-LAMP2 (The Burnham Institute, La Jolla, CA) and Dr. Colleen Fearns for critical feedback on the manuscript. This work was supported by the NIH (DK75295), the Skaggs Institute for Chemical Biology, and the Lita Annenberg Hazen Foundation. A.E.P. was supported by the NIH (GM084027).

References

1. Balch WE, Morimoto RI, Dillin A, Kelly JW. Adapting proteostasis for disease intervention. Science. 2008; 319:916–919. [PubMed: 18276881]
2. Deuerling E, Bukau B. Chaperone-assisted folding of newly synthesized proteins in the cytosol. Crit. Rev. Biochem. Mol. Biol. 2004; 39:261–277. [PubMed: 15763705]
3. Tang YC, Chang HC, Chakraborty K, Hartl FU, Hayer-Hartl M. Essential role of the chaperonin folding compartment in vivo. Embo J. 2008; 27:1458–1468. [PubMed: 18418386]
4. Bukau B, Weissman J, Horwich A. Molecular chaperones and protein quality control. Cell. 2006; 125:443–451. [PubMed: 16678092]
5. Morimoto RI, Cuervo AM. Protein Homeostasis and Aging: Taking Care of Proteins From the Cradle to the Grave. J. Gerontol. Ser.A-Biol. Sci.Med. Sci. 2009; 64A:167–170. [PubMed: 19228787]

Author Manuscript Author Manuscript Author Manuscript Author Manuscript

6. Westerheide SD, Anckar J, Stevens SM, Sistonen L, Morimoto RI. Stress-Inducible Regulation of Heat Shock Factor 1 by the Deacetylase SIRT1. Science. 2009; 323:1063–1066. [PubMed: 19229036]
7. Dai C, Whitesell L, Rogers AB, Lindquist S. Heat shock factor 1 is a powerful multifaceted modifier of carcinogenesis. Cell. 2007; 130:1005–1018. [PubMed: 17889646]
8. Ron D, Walter P. Signal integration in the endoplasmic reticulum unfolded protein response. Nat. Rev. Mol. Cell Biol. 2007; 8:519–529. [PubMed: 17565364]
9. Schroder M, Kaufman RJ. The mammalian unfolded protein response. Annu. Rev. Biochem. 2005; 74:739–789. [PubMed: 15952902]
10. Gidalevitz T, Ben-Zvi A, Ho KH, Brignull HR, Morimoto RI. Progressive disruption of cellular protein folding in models of polyglutamine diseases. Science. 2006; 311:1471–1474. [PubMed: 16469881]
11. Wang XD, et al. Hsp90 cochaperone Aha1 downregulation rescues misfolding of CFTR in cystic fibrosis. Cell. 2006; 127:803–815. [PubMed: 17110338]
12. Mu TW, Fowler DM, Kelly JW. Partial restoration of mutant enzyme homeostasis in three distinct lysosomal storage disease cell lines by altering calcium homeostasis. PloS. Biol. 2008; 6:253–265.
13. Mu TW, et al. Chemical and biological approaches synergize to ameliorate protein-folding diseases. Cell. 2008; 134:769–781. [PubMed: 18775310]
14. Cohen E, Bieschke J, Perciavalle RM, Kelly JW, Dillin A. Opposing activities protect against age-onset proteotoxicity. Science. 2006; 313:1604–1610. [PubMed: 16902091]
15. Morley JF, Brignull HR, Weyers JJ, Morimoto RI. The threshold for polyglutamine-expansion protein aggregation and cellular toxicity is dynamic and influenced by aging in Caenorhabditis elegans. Proc. Natl. Acad. Sci. USA. 2002; 99:10417–10422. [PubMed: 12122205]
16. Futerman AH, van Meer G. The cell biology of lysosomal storage disorders. Nat. Rev. Mol. Cell Biol. 2004; 5:554–65. [PubMed: 15232573]
17. Sawkar AR, et al. Chemical chaperones increase the cellular activity of N370S beta-glucosidase: a therapeutic strategy for Gaucher disease. Proc. Natl. Acad. Sci. U S A. 2002; 99:15428–33. [PubMed: 12434014]
18. Sawkar AR, D'Haeze W, Kelly JW. Therapeutic strategies to ameliorate lysosomal storage disorders - a focus on Gaucher disease. Cell. Mol. Life Sci. 2006; 63:1179–1192. [PubMed: 16568247]
19. Schmitz M, Alfalah M, Aerts J, Naim HY, Zimmer KP. Impaired trafficking of mutants of lysosomal glucocerebrosidase in Gaucher's disease. Int. J. Biochem. Cell Biol. 2005; 37:2310–2320. [PubMed: 15982918]
20. Ron I, Horowitz M. ER retention and degradation as the molecular basis underlying Gaucher disease heterogeneity. Hum. Mol. Genet. 2005; 14:2387–2398. [PubMed: 16000318]
21. Schueler UH, et al. Correlation between enzyme activity and substrate storage in a cell culture model system for Gaucher disease. J. Inherit. Metab. Dis. 2004; 27:649–658. [PubMed: 15669681]
22. Zimmer K-P, et al. Intracellular transport of acid β-glucosidase and lysosome-associated membrane proteins is affected in Gaucher's disease (G202R mutation). J. Path. 1999; 188:407–414. [PubMed: 10440752]
23. Sawkar AR, et al. Chemical chaperones and permissive temperatures alter the cellular localization of Gaucher disease associated glucocerebrosidase variants. ACS Chem. Biol. 2006; 1:235–251. [PubMed: 17163678]
24. Desnick RJ, Schuchman EH. Enzyme replacement and enhancement therapies: Lessons from lysosomal disorders. Nat. Rev. Genet. 2002; 3:954–966. [PubMed: 12459725]
25. Ohashi T, et al. Characterization of human glucocerebrosidase from different mutant alleles. J. Biol. Chem. 1991; 266:3661–3667. [PubMed: 1704891]
26. Korkotian E, et al. Elevation of intracellular glucosylceramide levels results in an increase in endoplasmic reticulum density and in functional calcium stores in cultured neurons. J. Biol. Chem. 1999; 274:21673–21678. [PubMed: 10419477]
27. Lloyd-Evans E, et al. Glucosylceramide and glucosylsphingosine modulate calcium mobilization from brain microsomes via different mechanisms. J. Biol.Chem. 2003; 278:23594–23599. [PubMed: 12709427]

Author Manuscript Author Manuscript Author Manuscript Author Manuscript

28. Pelled D, et al. Enhanced calcium release in the acute neuronopathic form of Gaucher disease. Neurobiol. Dis. 2005; 18:83–88. [PubMed: 15649698]
29. Valdivia HH, Valdivia C, Ma JJ, Coronado R. Direct binding of verapamil to the ryanodine receptor channel of sarcoplasmic-reticulum. Biophys. J. 1990; 58:471–481. [PubMed: 2169916]
30. Shoshanbarmatz V, Pressley TA, Higham S, Krausfriedmann N. Characterization of high-affinity ryanodine-binding sites of rat liver endoplasmic-reticulum - differences between liver and skeletal-muscle. Biochem. J. 1991; 276:41–46. [PubMed: 2039482]
31. Zalk R, Lehnart SE, Marks AR. Modulation of the ryanodine receptor and intracellular calcium. Annu. Rev. Biochem. 2007; 76:367–385. [PubMed: 17506640]
32. Ward A, Chaffman MO, Sorkin EM. Dantrolene - A review of its pharmacodynamic and pharmacokinetic properties and therapeutic use in malignant hyperthermia, the neuroleptic malignant syndrome and an update of its use in muscle spasticity. Drugs. 1986; 32:130–168. [PubMed: 3527659]
33. Kang JJ, Hsu KS, Linshiau SY. Effects of bipyridylium compounds on calcium-release from triadic vesicles isolated from rabbit skeletal-muscle. Br. J. Pharmacol. 1994; 112:1216–1222. [PubMed: 7952884]
34. Berridge MJ. Inositol trisphosphate and calcium signaling. Nature. 1993; 361:315–325. [PubMed: 8381210]
35. Vangheluwe P, Raeymaekers L, Dode L, Wuytack F. Modulating sarco(endo)plasmic reticulum Ca^{2+} ATPase 2 (SERCA2) activity: Cell biological implications. Cell Calcium. 2005; 38:291–302. [PubMed: 16105684]
36. Palmer AE, Jin C, Reed JC, Tsien RY. Bcl-2-mediated alterations in endoplasmic reticulum Ca^{2+} analyzed with an improved genetically encoded fluorescent sensor. Proc. Natl. Acad. Sci. USA. 2004; 101:17404–17409. [PubMed: 15585581]
37. Michalak M, Parker JMR, Opas M. Ca^{2+} signaling and calcium binding chaperones of the endoplasmic reticulum. Cell Calcium. 2002; 32:269–278. [PubMed: 12543089]
38. Schrag JD, et al. The structure of calnexin, an ER chaperone involved in quality control of protein folding. Mol. Cell. 2001; 8:633–644. [PubMed: 11583625]
39. Lamb HK, et al. The affinity of a major Ca^{2+} binding site on GRP78 is differentially enhanced by ADP and ATP. J. Biol. Chem. 2006; 281:8796–8805. [PubMed: 16418174]
40. Apperizeller-Herzog C, Ellgaard L. The human PDI family: Versatility packed into a single fold. Biochim. Biophys. Acta-Mol. Cell Res. 2008; 1783:535–548.
41. Wilson CM, Farmery MR, Bulleid NJ. Pivotal role of calnexin and mannose trimming in regulating the endoplasmic reticulum-associated degradation of major histocompatibility complex class I heavy chain. J. Biol. Chem. 2000; 275:21224–21232. [PubMed: 10801790]
42. Keller SH, Lindstrom J, Taylor P. Inhibition of glucose trimming with castanospermine reduces calnexin association and promotes proteasome degradation of the alpha-subunit of the nicotinic acetylcholine receptor. J. Biol. Chem. 1998; 273:17064–17072. [PubMed: 9642271]
43. Wang J, White AL. Role of calnexin, calreticulin, and endoplasmic reticulum mannosidase I in apolipoprotein(a) intracellular targeting. Biochemistry. 2000; 39:8993–9000. [PubMed: 10913312]
44. Brockmeier A, Williams DB. Potent lectin-independent chaperone function of calnexin under conditions prevalent within the lumen of the endoplasmic reticulum. Biochemistry. 2006; 45:12906–12916. [PubMed: 17042509]
45. Thammavongsa V, Mancino L, Raghavan M. Polypeptide substrate recognition by calnexin requires specific conformations of the calnexin protein. J. Biol. Chem. 2005; 280:33497–33505. [PubMed: 16061483]
46. Tjoelker LW, et al. Human, mouse and rat calreticulin cDNA cloning - identification of potential calcium-binding motifs and gene localization to human-chromosome-5. Biochemistry. 1994; 33:3229–3236. [PubMed: 8136357]
47. Corbett EF, et al. The conformation of calreticulin is influenced by the endoplasmic reticulum luminal environment. J. Biol. Chem. 2000; 275:27177–27185. [PubMed: 10842171]
48. Powers ET, Morimoto RI, Dillin A, Kelly JW, Balch WE. Biological and Chemical Approaches to Diseases of Proteostasis Deficiency. Annu. Rev. Biochem. 2009; 78:23.1–33.

Author Manuscript Author Manuscript Author Manuscript Author Manuscript

49. Le AQ, Steiner JL, Ferrell GA, Shaker JC, Sifers RN. Association between calnexin and a secretion-incompetent variant of human alpha(1)-antitrypsin. J. Biol. Chem. 1994; 269:7514–7519. [PubMed: 8125971]

50. David V, Hochstenbach F, Rajagopalan S, Brenner MB. Interaction with newly synthesized and retained proteins in the endoplasmic-reticulum suggests a chaperone function for human integral membrane-protein IP90 (calnexin). J. Biol. Chem. 1993; 268:9585–9592. [PubMed: 8486646]

Author Manuscript Author Manuscript Author Manuscript Author Manuscript

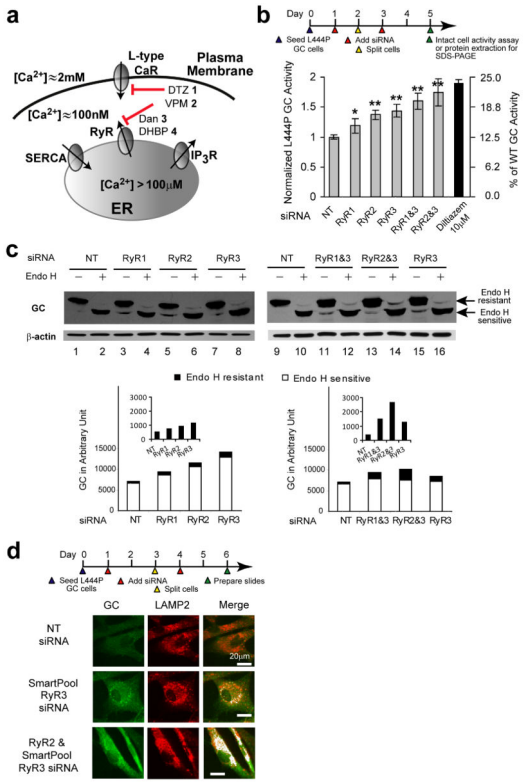

Figure 1.

siRNA-mediated knockdown of RyR isoforms partially restores L444P GC proteostasis. (**a**) Intra-ER Ca^{2+} concentration is regulated by L-type voltage-gated Ca^{2+} channels, ryanodine receptor (RyRs) Ca^{2+} efflux channels, IP_3 receptor Ca^{2+} efflux channels, and SERCA Ca^{2+} influx pumps. (**b**) Relative lysosomal GC activities of L444P fibroblasts upon single or double RyR1, RyR2 and RyR3 siRNA treatments, using the intact cell assay. Reported activities were normalized to the activity of cells treated with non-targeting siRNA (*, $p<0.01$; **, $p<0.001$). The experiments were repeated three times. The data are reported as mean ± SD. Statistical significance was evaluated using a two-tailed Student's t-Test. The diltiazem data has been reported previously12 and is included to enable comparison with RyR(s) siRNA treatment. (**c**) Western blot analysis of L444P fibroblast lysates without and with endo H treatment after the corresponding siRNA treatments. Co-application of siRNAs that target the RyR3 and another RyR isoform led to a significant increase in the endo H resistant post-ER GC glycoform bands in comparison to the non-targeting siRNA control. The white portion of the bars represents quantification (Java Image processing and analysis software from the NIH) of the lower, endo H sensitive bands, and the black portion of the bars represents the higher MW, endo H resistant post-ER glycoform. (**d**) Indirect immunofluorescence microscopy of GC in L444P fibroblasts reveals that the application of siRNA against RyR3 or siRNA against RyR2 and RyR3 enhances GC staining (green) and the colocalization between GC and LAMP2 (artificially colored white).

Author Manuscript Author Manuscript Author Manuscript Author Manuscript

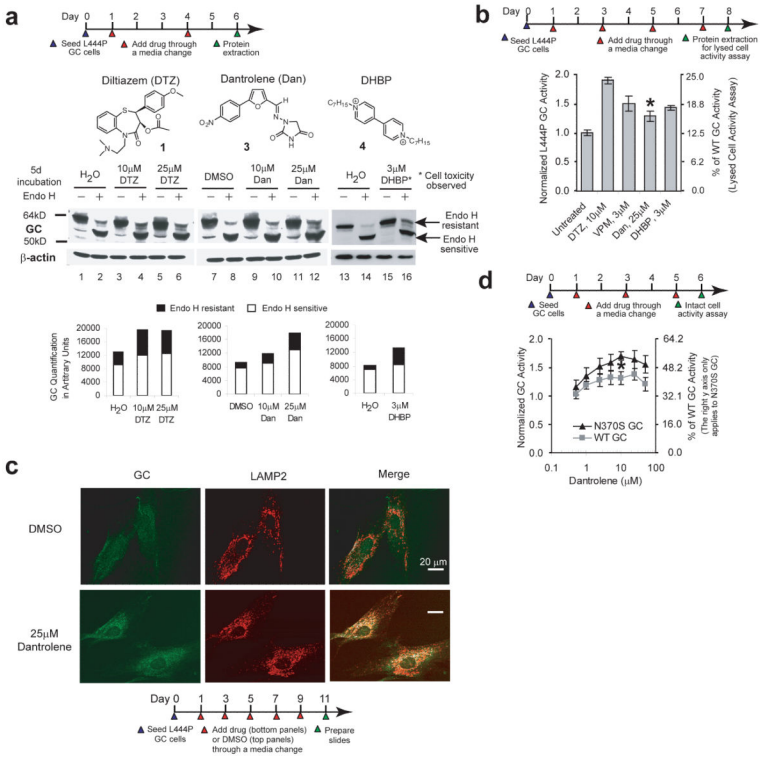

Figure 2.

Ryanodine receptor antagonists act as GC proteostasis regulators. (**a**) Small molecules that inhibit the RyRs enhance folding and trafficking of the L444P GC protein in L444P fibroblasts. The significant increase in endo H resistant post-ER GC glycoform when compared to the vehicle controls reflects increased GC proteostasis. Quantification of GC bands is shown in the bar graphs at the bottom of (**a**). (**b**) Diltiazem **1**, dantrolene **3** and DHBP **4** increase L444P GC enzyme activity (lysed cell activity assay), normalized to the vehicle controls (*, $p<0.001$). The verapamil **2** data, reported previously12, is included for comparison. (**c**) Indirect immunofluorescence microscopy of GC in L444P fibroblasts reveals that dantrolene **3** treatment enhances GC staining (green) and colocalization between GC and LAMP2 (artificially colored white). The experiments were repeated three times. (**d**) Dantrolene **3** increases WT and N370S GC enzyme activity (intact cell assay) in patient-derived fibroblasts, normalized to the vehicle control (*, $p<0.001$). Data in (**b**), and (**d**) are reported as mean ± SEM, statistical significance was evaluated using a two-tailed Student's t-Test.

Author Manuscript Author Manuscript Author Manuscript Author Manuscript

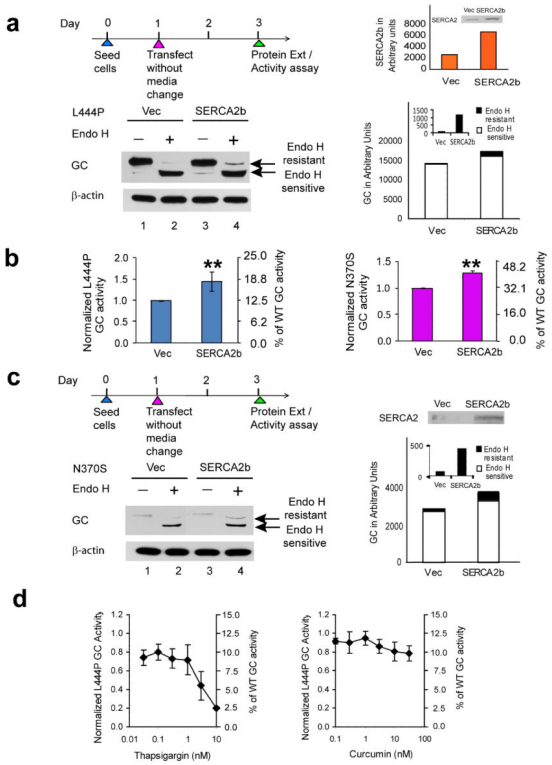

Figure 3.

Overexpression of the SERCA2b Ca^{2+} influx pump enhances mutant GC folding and trafficking. Transient overexpression of SERCA2b in L444P GC patient-derived fibroblasts for 2 d resulted in a significant increase in (**a**) the endo H resistant post-ER GC glycoform as well as (**b**) lysosomal GC enzyme activity (**, $p<0.001$) when compared to the empty vector control. An analogous increase in (**b**) lysosomal GC enzyme activity (**, $p<0.001$) and (**c**) endo H resistant post-ER GC glycoform band was also observed when SERCA2b was transiently overexpressed in N370S GC patient-derived fibroblasts. The L444P and N370S GC protein glycosylation pattern was analyzed by western blot analysis after endo H digestion as described in Fig. 1. The orange bars represent the level of SERCA2b expression in the fibroblasts. Incubation of the L444P fibroblasts with (**d**) thapsigargin **12**, a potent inhibitor of the SERCA2 pump, for 7 d significantly decreased the L444P GC lysosomal enzyme activity. All the experiments were repeated three times. Data in (**b**) and (**d**) are reported as mean ± SD. Statistical significance was evaluated using a two-tailed Student's t-Test.

Author Manuscript Author Manuscript Author Manuscript Author Manuscript

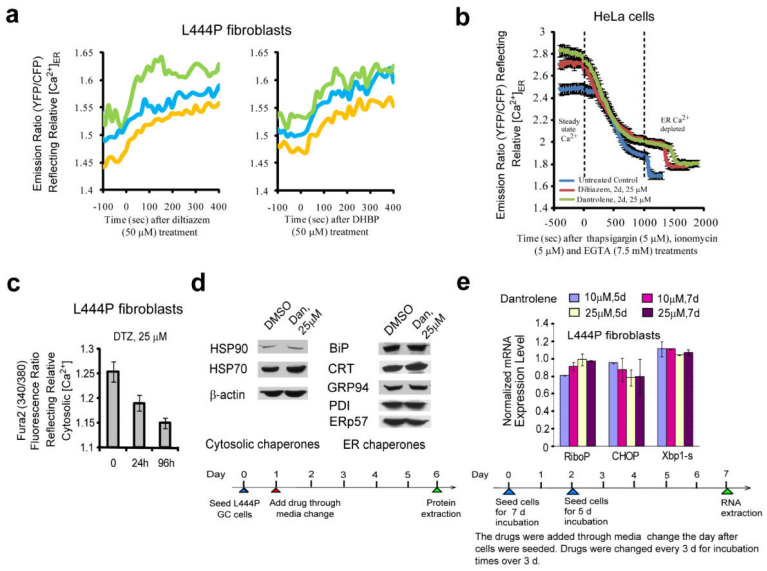

Figure 4.

Antagonists of the RyRs increase $[Ca^{2+}]_{ER}$ in fibroblasts and HeLa cells, but do not activate the HSR and UPR in the L444P fibroblasts. (**a**) Diltiazem **1** (50 μM) and DHBP **4** (50 μM) treatment increased the $[Ca^{2+}]_{ER}$ over the course of 400 sec in the L444P fibroblasts transfected with the D1-ER cameleon Ca^{2+} sensor 48 h prior. Each trace represents the time dependent emission ratio of YFP/CFP immediately after a single dose. (**b**) Two day treatment of HeLa cells with diltiazem **1** (25 μM) and dantrolene **3** (25 μM) increased the steady state $[Ca^{2+}]_{ER}$; revealed by first measuring the YFP/CFP ratio after 48 h treatment (drug-treated steady state Ca^{2+}) and second, by treatment with thapsigargin **12** (5 μM)/ ionomycin **15** (5 μM) and EGTA **16** (7.5 mM) to generate the ER Ca^{2+}-depleted state (minimum YFP/CFP ratio). The ER depletion time courses shown represent an average of 12 cells. (**c**) Diltiazem **1** (25 μM) decreased the steady state cytosolic Ca^{2+} levels in the L444P fibroblasts over a 1 and 4 d period using Fura2, AM. (**d**) Dantrolene **3** (25 μM) application does not activate the HSR or the UPR, based on western blot analysis of transcriptionally controlled chaperones and folding enzymes. (**e**) Dantrolene **3** (10 and 25 μM) does not activate the UPR based on qRT-PCR analysis of CHOP and spliced XBP-1. The large ribosomal protein, RiboP, serves as a housekeeping gene control. Data in (**b**), (**c**) and (**e**) are reported as mean ± SD.

Author Manuscript Author Manuscript Author Manuscript Author Manuscript

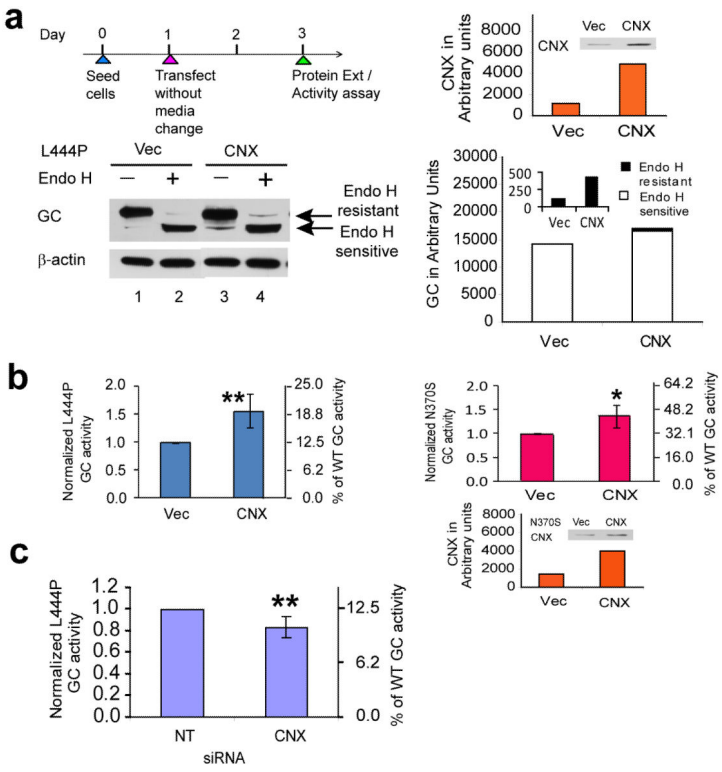

Figure 5.

Overexpression of calnexin partially restores mutant GC proteostasis. Transient overexpression of calnexin in the L444P GC patient-derived fibroblasts for 2 d resulted in a significant increase in (**a**) the endo H resistant post-ER GC glycoform bands as well as (**b**) lysosomal GC enzyme activity (**, $p<0.001$) when compared to the empty vector control. An analogous increase (*, $p<0.01$) in the (**b**) lysosomal GC enzyme activity was also observed when calnexin was transiently overexpressed in the N370S GC patient-derived fibroblasts. (**c**) The intact cell assay revealed a significant (**, $p<0.001$) decrease in the lysosomal L444P GC enzyme activity with calnexin knockdown. The L444P GC protein glycosylation pattern was analyzed by western blot analysis after endo H digestion as described in Fig. 1. The orange bars represent the level of calnexin expression in the fibroblasts. All the experiments were repeated three times. Data in (**b**) and (**c**) are reported as mean ± SD. Statistical significance was evaluated using a two-tailed Student's t-Test.

Author Manuscript Author Manuscript Author Manuscript Author Manuscript

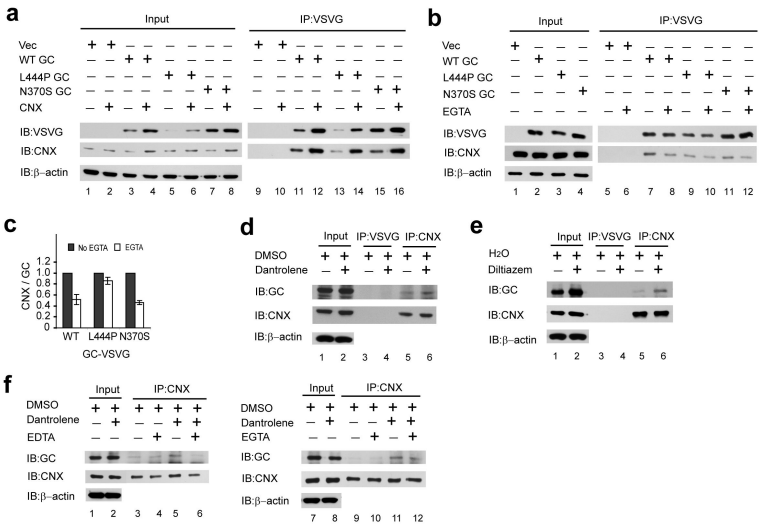

Figure 6.

The RyR antagonist category GC proteostasis regulators post-translationally regulate the chaperoning activity of calnexin in a Ca^{2+}-dependent manner. (**a**) Transient overexpression of calnexin and GC proteins in HeLa cells for 24 h resulted in a significant increase in the total WT, L444P and N370S GC proteins when compared to that with co-transfection of the GC and empty vector plasmids as revealed by western blot analysis. This was due to more calnexin being available to interact with the GC proteins. (**b**) The calnexin-GC protein interaction is Ca^{2+}-sensitive. Pre-incubation of the lysate with EGTA significantly reduced the calnexin-GC protein interaction. (**c**) After western blot analysis, the calnexin and GC protein bands were quantified using the ImageJ software (from NIH) and the bars represent the ratio of the calnexin to GC band intensities. The experiments were repeated three times. (**d**) Dantrolene **3** and (**e**) diltiazem **1** treatments increase the amount of L444P GC protein that is associated with calnexin, without increasing the calnexin protein level as revealed by western blot analysis. (**f**) Pre-incubating the RyR antagonist treated lysate with EDTA or EGTA significantly reduces the calnexin-GC protein interaction as revealed by western blot analysis. The experiments were repeated three times.